



# A novel route to obtain TiO<sub>2</sub> nanoparticles using green synthesis with vanillin and *Bougainvillea glabra Choisy* extract

María Concepción García-Castañeda<sup>1</sup> · Jesús Eduardo Castellanos-Águila<sup>2</sup> ·  
Geoffrey Humberto Israel Maury-Cuna<sup>3</sup> · Mónica Araceli Olea-Amezcuca<sup>4</sup> · Víctor Martín Escalante-Gómez<sup>5</sup> ·  
Rosalba Fuentes-Ramírez<sup>6</sup>

Received: 7 October 2020 / Accepted: 14 December 2020 / Published online: 31 January 2021  
© King Abdulaziz City for Science and Technology 2021

## Abstract

In this work, we present two green routes, as an alternative method to traditional synthesis, to obtain TiO<sub>2</sub> nanoparticles (NPs) from vanillin (TiO<sub>2</sub>\_V) and *Bougainvillea glabra Choisy* flower extracts (TiO<sub>2</sub>\_B) as suitable non-toxic reducing agents due to their potential to reduce their environmental impact and cost during the synthesis process. The NPs presented an anatase phase as confirmed by X-ray diffraction, and with crystallite sizes of 6.10 nm (TiO<sub>2</sub>\_V) and 5.89 nm (TiO<sub>2</sub>\_B), their hydrodynamic size and morphology were characterized by dynamic light scattering and scanning electron microscopy, respectively. Infrared spectroscopy confirmed TiO<sub>2</sub> characteristic bands for the obtained materials and from their UV–Vis absorption spectra band gap values of 3.07 and 3.08 eV for TiO<sub>2</sub>\_V and TiO<sub>2</sub>\_B, respectively, were calculated. Additionally, Grätzel cells were prepared to investigate the efficiency of the NPs obtained by this green synthesis. Finally, we included a theoretical section where, from ab initio calculations of structural and electronic properties, we explain the role of the reducing agents of the employed experimental synthesis, finding that the radicals restrict the grown-up of the clusters by the passivation of the dangling bonds modifying the crystal structure of the clusters splitting the  $t_{2g}$  orbitals, altering the band gap of the clusters.

**Keywords** Green synthesis · Titanium dioxide · Photoenergy · DFT · Theoretical properties

**Supplementary Information** The online version contains supplementary material available at <https://doi.org/10.1007/s13204-020-01648-9>.

✉ María Concepción García-Castañeda  
mgarciaca@ugto.mx

Jesús Eduardo Castellanos-Águila  
je.castellanos@ugto.mx

Geoffrey Humberto Israel Maury-Cuna  
israel.maury@ugto.mx

Mónica Araceli Olea-Amezcuca  
monica.olea@correo.buap.mx

Víctor Martín Escalante-Gómez  
escalantegv@gmail.com

Rosalba Fuentes-Ramírez  
rosalba@ugto.mx

<sup>1</sup> CONACyT-Universidad de Guanajuato, Loma del Bosque 103, Col. Lomas del Campestre, C. P. 37150 León, Guanajuato, Mexico

<sup>2</sup> Departamento de Estudios Multidisciplinarios, Universidad de Guanajuato, Av. Yacatitas, S/N Col. Yacatitas, C. P. 36940 Yuriria, Guanajuato, Mexico

<sup>3</sup> Departamento de Física, División de Ciencias e Ingenierías, Universidad de Guanajuato, Loma del Bosque 103, Col. Lomas del Campestre, C. P. 37150 León, Guanajuato, Mexico

<sup>4</sup> Escuela de Artes Plásticas y Audiovisuales, Benemérita Universidad Autónoma de Puebla, Vía Atlixcáyotl 2499, C.P. 72810 Puebla, Puebla, Mexico

<sup>5</sup> División de Ciencias e Ingenierías, Loma del Bosque 103, Col. Lomas del Campestre, C. P. 37150 León, Guanajuato, Mexico

<sup>6</sup> División de Ciencias Naturales y Exactas, Universidad de Guanajuato, Noria Alta S. N., C. P. 36050 Guanajuato, Guanajuato, Mexico

## Introduction

The synthesis of nanoparticles (NPs) of metals and metal oxides is of great importance due to its many applications, and it proposes benefits of almost any nature, from medical, technological uses, or benefits to the environment. The properties shown by nanomaterials compared to the bulk properties have produced a new generation of materials with extraordinary physical and chemical properties, causing the area of nanotechnology primarily focused on TiO<sub>2</sub> nanoparticles to encompass a growing scope in the last decades. Among the most studied nanomaterials, metal oxide nanoparticles are of particular interest due to their multifunctional capabilities (Ibarra 2015); specifically, the TiO<sub>2</sub> nanoparticles have a large specific surface area and a high surface activity when they are on the nanometric scale (Hussain et al. 2010). The preparation of the NPs of this metal oxide has been thoroughly investigated using various synthesis methods with which the final properties can be affected depending on the morphology and the formation of agglomerates (Dubey et al. 2019).

In the production of nanomaterials, there is a growing concern about the generation of toxic waste that is potentially harmful to humans and the environment. One option to address this problem is to apply the principles of green chemistry to synthesize these materials. In this context, plant extracts provide a new biosynthetic route capable of achieving quality products that are non-toxic to humans and the environment. According to those mentioned above, there is considerable interest in the antioxidant properties present in organic compounds and secondary metabolites of different plant species, such as polyphenols, phenolic acids, and flavonoids. Consequently, studies have recently begun to produce nanostructures from extracts or essential oils that allow reducing metal salts. The vanillin structure (4-hydroxy-3-methoxybenzaldehyde) is a compound derived from phenolic acids, which has a hydroxyl, ether, and aldehyde radical present in the vanilla bean, but which can also be obtained by synthetic methods from lignin or guaiacol (Kumar et al. 2012). A study of pulsed radiation with radiolytic species showed that vanillin had reducing properties in some biomolecules due to the formation of phenolate ions that could relocate an electron in the molecule or transfer it, forming phenoxy radicals at higher values of pH (Mahal et al. 2001).

Furthermore, the composition and quantity of organic compounds or metabolites present in the bougainvillea plant depend on the extraction conditions, mainly on characteristics such as the genus of the species, the plant section where the extraction is carried out, and the polarity of the solvent used. In the particular case of *B. glabra*, compounds corresponding to flavonoids, sterols, terpenes,

carbohydrates, and betalains have been found in ethanolic extractions (Abarca-Vargas and Petricevich 2018). The latter implies a higher concentration of OH and C=O functional groups, which have reducing properties that also act as stabilizing/capping agents in the biosynthesis of nanomaterials and that could ultimately impact the final characteristics of materials such as shape and size (Arief et al. 2017; Rauf et al. 2019).

In this work, as an alternative to the traditional synthesis, we present two green routes to obtain TiO<sub>2</sub> NPs from vanillin and *Bougainvillea glabra* Choisy flower extracts as suitable non-toxic reducing agents, with the potential to reduce their environmental impact and cost during the synthesis process. Also, we include a theoretical study to determine the effect of the OH<sup>-</sup> radicals on the morphology and optical properties of the particles obtained.

## Experimental section

### Preparation of bougainvillea extract and vanillin solution

The bougainvillea flowers were washed with distilled water and dehydrated for 72 h at 65 °C; subsequently, they were grinded to obtain a powder. For the specific case of bougainvillea, 15 g of the powder obtained from the flowers were required, which were refluxed with 150 mL of isopropanol. The system was kept under stirring for 1 h at a temperature of 60 °C. On the other hand, food-grade vanillin powder (4-hydroxy-3-methoxybenzaldehyde) was purchased, and directly dissolved in 150 mL of isopropanol and stirred for 1 h at 60 °C. Both samples separately were filtered at room temperature (23 °C and relative humidity of 56%) using Whatman No. 1 filter paper.

### Preparation of TiO<sub>2</sub> nanoparticles

The synthesis process used 0.6 mL of the vanillin solution and the bougainvillea extract. For each case, 0.5 mL of HNO<sub>3</sub> was added in 60 mL of deionized water, leaving stirring at room temperature for 1 h. After this time, titanium isopropoxide (TTIP, Ti[OCH(CH<sub>3</sub>)<sub>2</sub>]<sub>4</sub>) with purity 97% (Sigma-Aldrich) was added, and the system was refluxed at 80 °C for 1 h. After synthesis, the solutions were centrifuged for 30 min at 4000 rpm to decant the aqueous phase and remove the TiO<sub>2</sub> NPs, which were dried at 70 °C for 24 h. The green synthesis was carried out without the calcination process, and the particles obtained by this method were ground in an agate mortar to separate most of the agglomerated particles.

The sample of TiO<sub>2</sub> anatase (TiO<sub>2</sub>\_A), which was used as a reference, was synthesized by the hydrothermal method reported by Tong et al. (2008).

### Characterization of TiO<sub>2</sub> nanoparticles

The particles synthesized by the three different methods were characterized for the investigation of their crystalline phases and the size of the crystals using X-ray diffraction (Bruker D2 Phaser), the hydrodynamic size was measured using the technique of dynamic light scattering (NanoFlex); the morphology of the samples was analyzed in a scanning electron microscope (JEOL JSM-7800F). Optical measurements were carried out on a UV–Vis spectrometer equipped with an integrating sphere (Agilent Mod. Cary 6000i UV–Vis–NIR), and by infrared spectroscopy (Agilent Cary 600) was analyzed the chemical structure of TiO<sub>2</sub>.

### Preparation of Grätzel cells

For the preparation of Grätzel cells, it was necessary to dissolve the TiO<sub>2</sub> samples in a 10% HCl solution. Later on, this paste was deposited by blade coating method in three stacked layers on the conductive FTO glass (Solaronix 15 Ω/sq), with dimensions of 25 × 25 × 2 mm; subsequently, it was sintered in a muffle at 450 °C for 1 h. To sensitize the samples, we employed an N719 standard dye solution dissolved in 100 mL of acetonitrile (both reagents Sigma-Aldrich brand). For the counter electrode, a glass coated with a solution of hexachloroplatinic acid hexahydrate (H<sub>2</sub>Cl<sub>6</sub>Pt·6H<sub>2</sub>O) in isopropanol was used, which was heat-treated at 450 °C for 30 min. Finally, the composition of the redox mediator used was Sigma Aldrich brand 0.3 M lithium iodide (99% purity) and 0.015 M elemental iodine (I<sub>2</sub> 99.8–100.5%, Reasol), which was dissolved in carbonate of propylene (CP 99.7%, Aldrich). The cell efficiency was determined using a light source with a photon flux of 72.5 mW/cm<sup>2</sup> at 15 cm from the sample and an incidence angle of 90°.

### Theoretical section

To understand the effects of the environment generated by the experimental proposed synthesis methods on the electronic properties of the nanoparticles, we constructed several titanium dioxide anatase clusters, (TiO<sub>2</sub>)<sub>n</sub> (n = 4, 8, 16, 32, 36, 72, 108). All the clusters were computed under three different schemes, considering the number of OH<sup>−</sup> radicals around each system: (0-OH), (6-OH) and (12-OH). The latter was done to mimic the behaviour of the employed green synthesis, since the OH<sup>−</sup> radicals are the reducing agents of this method. All the calculations were performed using the Density Functional Theory (DFT) as is implemented in

the Vienna ab initio simulation package (VASP) (Kresse and Furthmüller 1996). The core-valence interactions were described by the frozen-core projector augmented wave (PAW) method (Blöchl 1994; Kresse and Joubert 1999). Soft PAW potentials were used for Ti and O atoms. The wavefunctions were expanded in plane waves with an energy cut-off of 400 eV. We considered only  $\Gamma$ -point sampling of the Brillouin zone. Van der Waals corrections have been applied to total energies and forces through the DFT–D3 method (Grimme et al. 2011). In Fig. 1, we present the titanium dioxide cluster (TiO<sub>2</sub>)<sub>108</sub> without radicals. For the cases of the (6-OH) and (12-OH) schemes, the radicals were placed around the nanoparticles.

Considering that nanoparticles are finite systems, one could not define the true band gaps because of the high surface-to-volume ratio; the properties behave differently in both limits. To approach this situation, in the first step, we employed a supercell model with one nanoparticle of (TiO<sub>2</sub>)<sub>n</sub> per unit cell. To avoid spurious interactions between periodic images, we considered a vacuum of ~ 16 Å in all three directions. Once we have obtained relaxed structures, we proceed to calculate the band gap of a representative bulk, built from the corresponding volumetric deformations suffered by each nanoparticle under the effects of the simulated environments. In addition, the hybrid functional HSE was included in the calculations (Heyd et al. 2006). We used a proportion of ~ 20% of HF exchange with 80% PBE exchange to obtain accurate energy values for the band gaps (Ünal et al. 2015).

### Experimental results

The crystalline phase of the synthesized particles was studied by XRD. Figure 2 exhibits the TiO<sub>2</sub> patterns of samples A (anatase), B (bougainvillea) and V (vanillin), recorded at room temperature in 2θ angle in the range of 20–70 °C using CuKα radiation (λ = 0.15406 nm). The diffraction patterns on (101), (103), (004), (200), (105), (211) and (213) were found to be consistent with the reflections of anatase phase

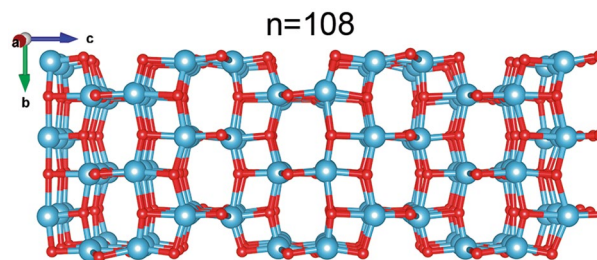


**Fig. 1** (TiO<sub>2</sub>)<sub>108</sub> anatase supercell where blue spheres are titanium atoms and red spheres are oxygen atoms. Similar structures are employed to simulate the different proposed nanoparticles

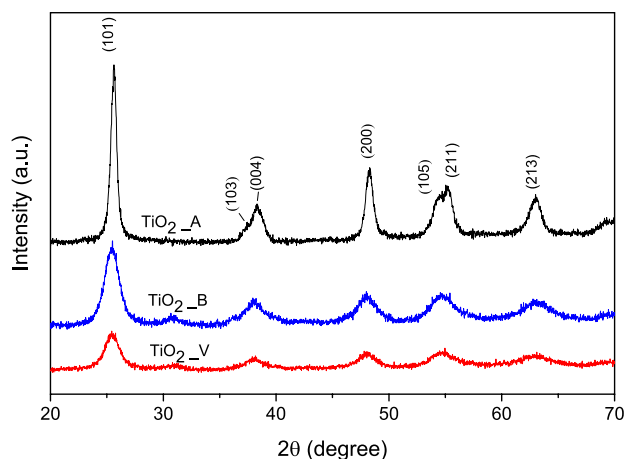


**Fig. 2** X-ray diffraction (XRD) pattern of synthesized TiO<sub>2</sub> NPs

of TiO<sub>2</sub> in accordance with JCPDS card No. 21–1272 (Al-Taweel and Saud 2016; Godbert et al. 2018; Goutam et al. 2018). The syntheses made with vanillin and bougainvillea extract (TiO<sub>2</sub>\_V and TiO<sub>2</sub>\_B respectively), showed the same diffraction peaks even without a calcination treatment after the synthesis (Watson et al. 2004). However, the length and sharpness of the diffraction patterns are related to the calcination temperatures (He et al. 2014) and the storage time. Furthermore, the signal at  $2\theta = 25.30^\circ$  implies the presence of the anatase phase only, which for the TiO<sub>2</sub>\_A sample is more defined because it was calcined at 400 °C (Liu et al. 2012).

The size of the crystals showed in Table 1, was calculated using the maximum peak and according to the Debye–Scherrer equation  $d = k\lambda/\beta\cos\theta$ , where  $k$  is a constant of the shape factor,  $\lambda$  is the wavelength of the X-ray radiation and  $\beta$  is the full width of the peak at half height (Al-Taweel and Saud 2016).

In Fig. 3, the results obtained by dynamic light scattering (DLS) are shown, for the particles obtained by the three synthesis methods. The particles obtained by the hydrothermal method (TiO<sub>2</sub>\_A), presented a broad monomodal signal in the 1500 nm zone that would be representing 93% of the total volume of the dispersed phase while the samples obtained by green routes are in the order of 300 nm for the highest percentage of their volume in the dispersed

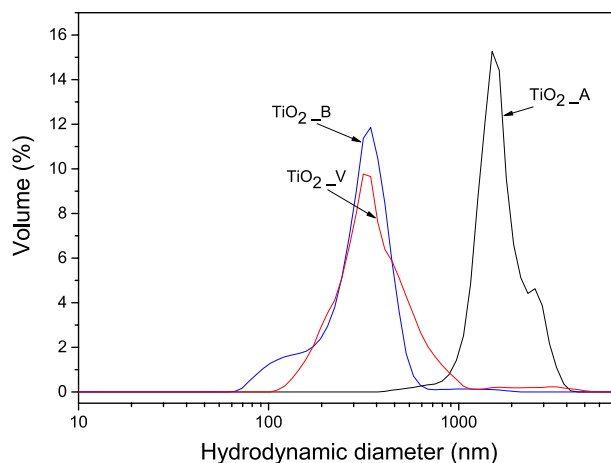


**Fig. 3** Dynamic light scattering (DLS) measurements of size dispersion of the TiO<sub>2</sub> particles obtained from different synthesis

phase. The size of the particles obtained by DLS is larger than measurements by other techniques since they are not of individual particles but of large agglomerates dispersed in an aqueous medium; these are generated as a consequence of their ability to attract each other due to its high surface energy (Hafizah and Iis 2009).

Figure 4 shows SEM micrographs of the synthesized NPs. TiO<sub>2</sub>\_V sample showed a morphology similar to the traditional synthesis due to electrostatic forces on their surface and the presence of metabolites as reported by Shanavas et al. (2019). Conversely, the TiO<sub>2</sub>\_B sample presented an irregular plate-like morphology; Amanulla and Sundaram (2019) reported a similar effect with NPs synthesized from plant extracts. A possible explanation for the latter case is that an excess of OH radicals (systems with  $n > 16$ , as reported in the Theoretical Section) generates a volumetric deformation leading to a relaxation in the clusters, which gives place to an irregular morphology.

The presence of functional groups was analysed using FTIR as shown in Fig. 5. The FTIR spectrum of vanillin powder (Fig. 5a) shows characteristic signals at 1590, 1510, and 731 cm<sup>-1</sup> corresponding to vibrations of the C=C stretch of the aromatic ring. In comparison, the 1660 cm<sup>-1</sup> signal corresponds to a stretching of the C=O bond of the aldehyde group. The band located at 3163 cm<sup>-1</sup> is attributed to an –O–H stretch belonging to a phenolic group. Whereas the signals at 1660 and 1150 cm<sup>-1</sup> are stretches of the C=O and C–O–C bonds, respectively (Shekarforoush et al. 2017). On the other hand, the powder of *B. glabra* flower presented a broad signal between 3400 and 3100 cm<sup>-1</sup> characteristic of the –O–H groups. Finally, the signals at 1726, 1610, and 1023 cm<sup>-1</sup> correspond to the stretching absorption vibrations of the C=O, C=C, and –C–O bonds, respectively. In Fig. 5b, we can observe broad and small peaks in 3400 cm<sup>-1</sup> and a 1640 cm<sup>-1</sup>, were assigned for stretching and bending

**Table 1** Comparison of different size samples (DLS, SEM and XRD)

Sample	DLS (nm)	SEM (nm)	Crystal-lite size (nm)
TiO <sub>2</sub> _A	1500	800	14.76
TiO <sub>2</sub> _B	342	400	5.89
TiO <sub>2</sub> _V	325	500	6.10

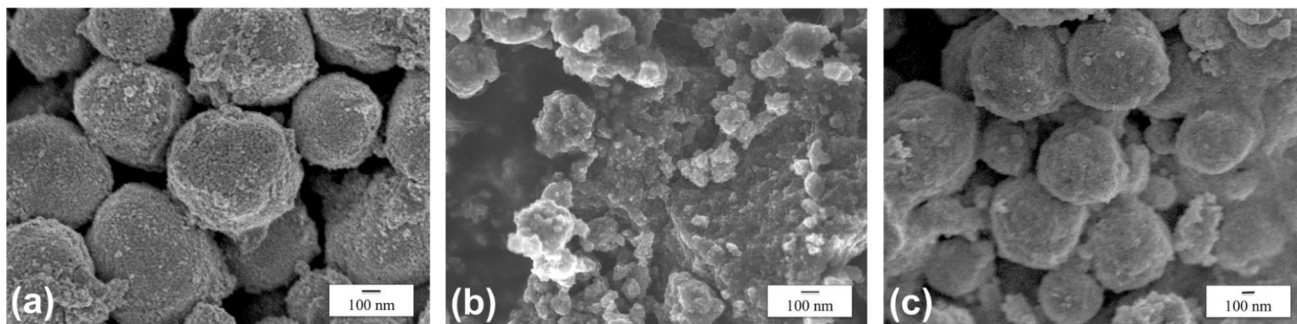


Fig. 4 SEM images of a TiO<sub>2</sub>\_A, b TiO<sub>2</sub>\_B and c TiO<sub>2</sub>\_V

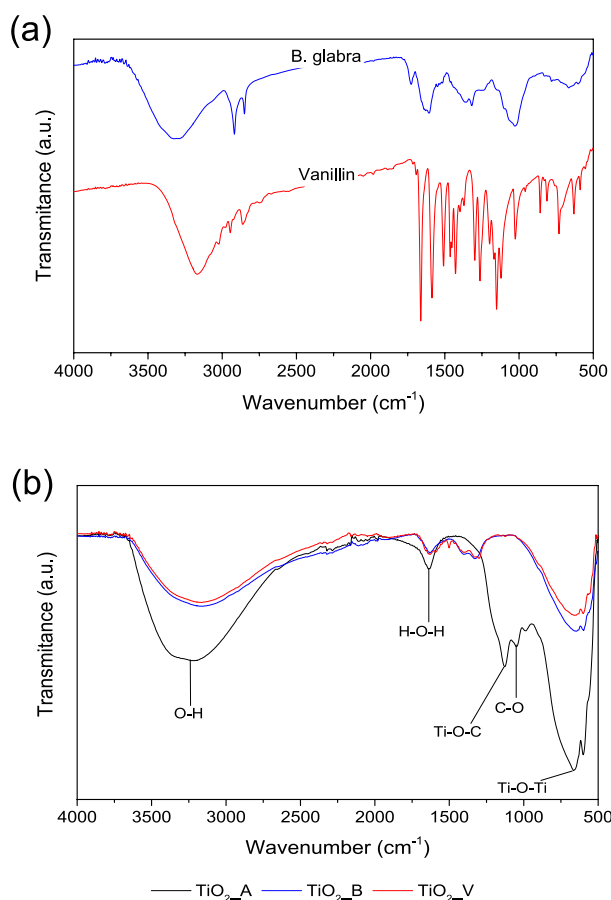


Fig. 5 FTIR spectrum of a Vanillin and Bougainvillea glabra powder and b different TiO<sub>2</sub> synthesized

vibrations respectively from hydroxyl groups and water molecules present on the TiO<sub>2</sub> surface. The presence of -OH groups is related to photocatalytic properties of TiO<sub>2</sub> NPs (Goutam et al. 2018; Amanulla and Sundaram 2019). Two bands in 1045 and 1130 cm<sup>-1</sup> were ascribed for C–O–Ti vibration bond (Ochoa et al. 2010; Amanulla and Sundaram 2019). Between 500 and 700 cm<sup>-1</sup> a broad peak corresponds to Ti–O stretching and Ti–O–Ti bridging stretching

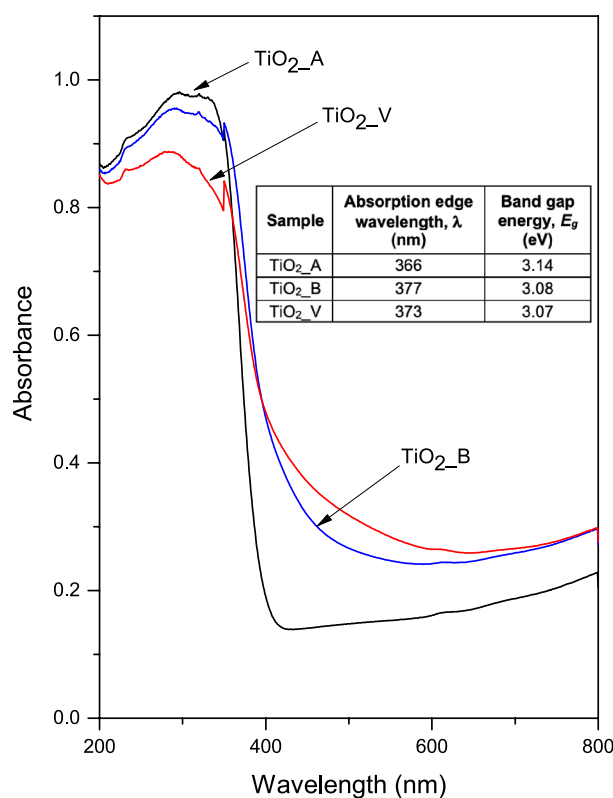


Fig. 6 UV-Vis spectra of TiO<sub>2</sub> samples and its band gap values

frequencies. Both TiO<sub>2</sub> green syntheses presented a small peak near 1420 cm<sup>-1</sup> attributed to the presence of -OH groups coming from secondary metabolites which form a complex with the metal ion (Marslin et al. 2018); nevertheless, this peak could disappear after an annealing process as reported by Liu et al. (2012).

An analysis of the absorption spectra was carried out to study the optical properties of the TiO<sub>2</sub> NPs, and to determine the prohibited energy band. Based on the minimum absorption energy necessary to promote the electrons from the valence band to the conduction band, we used the Tauc

method with the correction proposed by Makula et al. (2018). This method was applied to the spectrum obtained by UV–Vis (Fig. 6); in addition, the absorbance was calculated applying the first-derivative method to the same spectrum to calculate the inflection point. The band gap energy ( $E_g$ ) calculated for each sample is shown in the embedded table in Fig. 6, the absorption of photons of energy higher than  $E_g$ , better known as photoexcitation, promotes electrons from the valence band to the conduction band, which will define their possible uses and applications. The difference among the band gap values obtained is a consequence of wider absorption bands due to the presence of secondary metabolites on the NPs surface capable of absorbing higher wavelengths.

Grätzel cells were prepared to measure the performance of the TiO<sub>2</sub> materials by comparing their characteristic  $I$ – $V$  curves of each sample (Fig. 7). The low efficiencies of the cells prepared using the green NPs, are attributed to a reduction in the photo-response of TiO<sub>2</sub> due to inadequate absorption of the dye (Jeng et al. 2013). The low values of  $J_{sc}$  and FF, shown in the table embedded in Fig. 7, are a consequence of the preparation method used due to limited control over the thickness of the TiO<sub>2</sub> layers in the photoelectrode. A refinement in the preparation technique and choosing of suitable dope materials could improve these values for further research (Ruhane et al. 2017; Sharma et al. 2018).

## Theoretical results

Returning to the objective of the theoretical contribution in this work, to understand the role of the green reduction agents on the structural configuration and electronic band gaps of the NPs, we performed a systematical analysis of

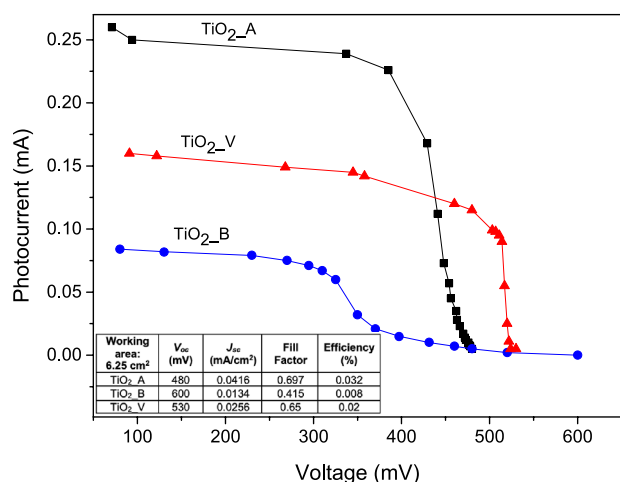


Fig. 7 V–I Grätzel cells curve

the several clusters under different environments, taking as a reference point the respective calculated values for the TiO<sub>2</sub> bulk. So, we took the system with 6 OH<sup>−</sup> radicals as a representation of the experimental vanillin green synthesis, since the bougainvillea extract method presents more OH<sup>−</sup> radicals, the (12-OH) scheme represents it. In this way, we present in Table S1 (see the Supporting Information) the unit cell volume values and the  $E_g$ , for each theoretical system proposed. In general, for systems with  $n < 16$ , the interaction between the nanocluster and the OH<sup>−</sup> radicals compress the cluster, as a consequence, the internal atoms of the nanoparticles are stressed. Inversely, systems with  $n > 16$  show a slight increase in total volume.

For a visual simplification, we present in the Fig. 8 the band gap value as a function of the volumetric deformation,  $\delta$ . This figure and Table S1 show the well-known behaviour of band gap values with respect to the volume, the inverse relationship between them (Monticone et al. 2000; Choudhury and Choudhury 2014). According to our results, the presence of different gradients of OH<sup>−</sup> radicals concentration generates several volumetric deformations and, therefore, a variation on the band gap values.

To understand the origin of the band gap variations in the TiO<sub>2</sub> systems, we performed an analysis of the density of states for all nanoclusters (depicted in the Supplemental Information). We corroborate that O-2*p* states predominantly form the top of the valence bands; meanwhile, the bottom of the conduction bands consists of the Ti-3*d* states, which are responsible for the band gap variations. Additionally, we developed a PDOS analysis for all systems; in the Fig. 9, we present the case of the

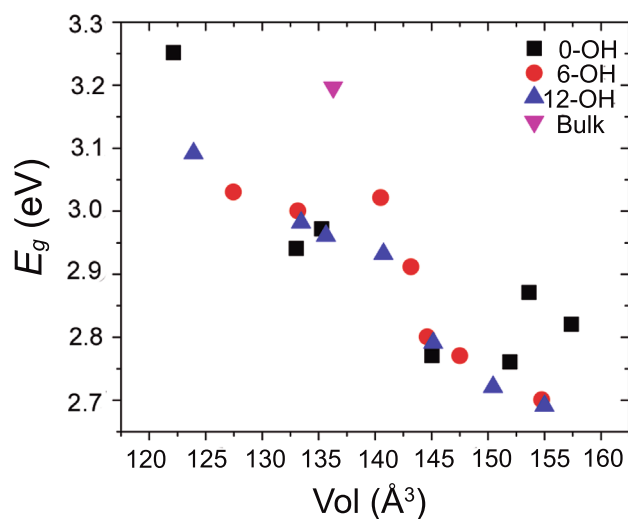
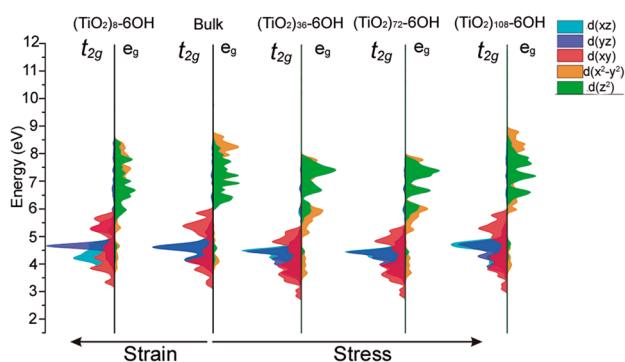


Fig. 8 Calculated energy band gaps for all the proposed systems under study in comparison to the bulk ones under the vacuum and OH<sup>−</sup> radicals schemes. Lines are a guide to eye. Experimental data is indicated by horizontal red line



**Fig. 9** PDOS of  $\text{TiO}_2$  with 6  $\text{OH}^-$  radicals around each system. The DOS is decomposed into Ti  $t_{2g}$  ( $d_{xy}$ ,  $d_{yz}$ , and  $d_{xz}$ ), and Ti  $e_g$  ( $d_x^2 - y^2$ , and  $d_z^2$ ). The PDOS calculated for the other systems are showed in the Supporting Information

6  $\text{OH}^-$  radicals to discuss the general behaviour of the different splittings of the  $t_{2g}$  and  $e_g$  orbitals of the  $\text{TiO}_2$  nanoclusters, which are directly correlated to the structural distortion present in the nanoclusters. In the first place, we can see that the main contribution to the changes in the band gap values is determined by the  $t_{2g}$  states. In a perfect octahedral system, like  $\text{TiO}_2$  in the anatase phase, the  $d_{xz}$  and  $d_{yz}$  orbitals are degenerate. When our systems are deformed, the octahedral environment is broken, and the  $d_{xz}$  and  $d_{yz}$  orbitals split. On the other hand, the  $d_{xy}$  orbitals are responsible for the band gap variations because they are in the edges of the conduction bands.

Finally, to evaluate the dependency of the structural configuration of the different clusters on the green synthesis method, we calculated the formation energy for each case (depicted in the Supplemental Information) (Batzill et al. 2006; Pabisiak and Kiejna 2007). In all the cases, the obtained values were negative and are in the energy range of the 2.68–17.48 eV. In this band gap range, of values it is difficult to assign to the type of interaction, because this energy depends on the nanoparticle size, which influences the interaction between  $\text{OH}^-$  radicals and on the possible passivation of the dangling bonds by the formation of two types of bonds (Ti–O–H or O–O–H), preventing the growth of the clusters. In general, the biggest nanoparticles are energetically less affected by the presence of the  $\text{OH}^-$  radicals.

Summing up, we find that the  $\text{OH}^-$  radicals play an essential role to tune the electronic properties in the nanosystems studied here. According to the theoretical results, the size can be controlled with the green reduction agents, where the  $\text{OH}^-$  radicals restrict the grown-up of the clusters by the passivation of the dangling bonds modifying the crystal structure of the clusters which splits the  $t_{2g}$  orbitals, resulting in a modification of the conduction band. This passivation, from the experimental view, can be interpreted as the interruption of the agglomeration.

## Conclusions

Vanillin and *Bougainvillea glabra* Choisy flower extracts were employed as metal ion reducing agents to successfully obtain  $\text{TiO}_2$  nanoparticles by a simple green synthesis method. X-ray diffraction showed the characteristic patterns of the anatase phase without the need for calcination. A band related to the formation of an ion-metal complex was found by FTIR. Finally, the UV–Vis spectra band gap values are within the characteristic range for the  $\text{TiO}_2$  anatase phase. To simulate the effects of the reducing agents in the green method synthesis, first-principle calculations were performed to investigate the electronic and structural responses of different sizes of nanoparticles under the influence  $\text{OH}^-$  radicals' concentration. We conclude that the NPs crystal structure varies with respect to the concentration of the radicals by the passivation of certain dangling bonds, which is reflected in the electronic properties, such as those shown by the analysis of the PDOS. For each proposed system, the splitting of  $t_{2g}$  orbitals of the  $\text{TiO}_2$  is observed resulting in a band gap variation.

## Compliance with ethical standards

**Conflict of interest** On behalf of all authors, the corresponding author states that there is no conflict of interest.

## References

- Abarca-Vargas R, Petricevich VL (2018) *Bougainvillea* genus: a review on phytochemistry, pharmacology, and toxicology. *Evid Based Complem Alternat Med* 2018:1–17. <https://doi.org/10.1155/2018/9070927>
- Al-Taweel S, Saud H (2016) New route for synthesis of pure anatase  $\text{TiO}_2$  nanoparticles via ultrasound-assisted sol-gel method. *J Chem Pharm Res* 8:620–626
- Amanulla AM, Sundaram R (2019) Green synthesis of  $\text{TiO}_2$  nanoparticles using orange peel extract for antibacterial, cytotoxicity and humidity sensor applications. *Mater Today Proc* 8:323–331. <https://doi.org/10.1016/j.matpr.2019.02.118>
- Arief S, Hidayani P, Aferta L, Zulhadjri Ban T, Ohya Y (2017) Green chemistry formation of stable Ag nanoparticles (AgNPs) in isopropanol solvent. *Orient J Chem* 33(1):87–91. <https://doi.org/10.13005/ojc/330109>
- Batzill M, Morales EH, Diebold U (2006) Influence of nitrogen doping on the defect formation and surface properties of  $\text{TiO}_2$  rutile and anatase. *Phys Rev Lett* 96:026103. <https://doi.org/10.1103/PhysRevLett.96.026103>
- Blöchl PE (1994) Projector augmented-wave method. *Phys Rev B* 50:17953. <https://doi.org/10.1103/PhysRevB.50.17953>
- Choudhury B, Choudhury A (2014) Oxygen defect dependent variation of band gap, Urbach energy and luminescence property of anatase, anatase-rutile mixed phase and of rutile phases of  $\text{TiO}_2$  nanoparticles. *Phys E* 56:364–371. <https://doi.org/10.1016/j.physe.2013.10.014>

- Dubey R, Krishnamurthy KV, Singh S (2019) Experimental studies of TiO<sub>2</sub> nanoparticles synthesized by sol-gel and solvothermal routes for DSSCs application. *Res Phys* 14:102390. <https://doi.org/10.1016/j.rinp.2019.102390>
- Godbert N, Mastropietro T, Poerio T (2018) Mesoporous TiO<sub>2</sub> thin films: state of the art. <http://doi.org/10.5772/intechopen.74244>
- Goutam SP, Saxena G, Singh V, Yadav AK, Bharagava RN, Thapa KB (2018) Green synthesis of TiO<sub>2</sub> nanoparticles using leaf extract of *Jatropha curcas* L. for photocatalytic degradation of tannery wastewater. *Chem Eng J* 336:386–396. <https://doi.org/10.1016/j.cej.2017.12.029>
- Grimme S, Ehrlich S, Goerigk L (2011) A consistent and accurate ab initio parametrization of density functional dispersion correction (DFT-D) for the 94 elements H–Pu. *J Comp Chem* 32:1456. <https://doi.org/10.1063/1.3382344>
- Hafizah N, Iis S (2009) Nanosized TiO<sub>2</sub> photocatalyst powder via sol-gel method: effect of hydrolysis degree on powder properties. *Int J Photoenergy* 2009:1–8. <https://doi.org/10.1155/2009/962783>
- He F, Ma F, Li J, Li T, Li G (2014) Effect of calcination temperature on the structural properties and photocatalytic activities of solvothermal synthesized TiO<sub>2</sub> hollow nanoparticles. *Ceram Int* 40:6441–6446. <https://doi.org/10.1016/j.ceramint.2013.11.094>
- Heyd J, Scuseria GE, Ernzerhof M (2006) Erratum: “Hybrid functionals based on a screened Coulomb potential” [*J. Chem. Phys.* 118, 8207 (2003)]. *J Chem Phys* 124:219906. <https://doi.org/10.1063/1.2204597>
- Hussain M, Ceccarelli R, Marchisio D, Fino D, Russo N, Geobaldo F (2010) Synthesis, characterization and photocatalytic application of novel TiO<sub>2</sub> nanoparticles. *Chem Eng J* 157:45–51. <https://doi.org/10.1016/j.cej.2009.10.043>
- Ibarra JJ (2015) Síntesis de nanopartículas de plata y dióxido de titanio por métodos ambientalmente amigables para aplicaciones en la industria de la curtiduría. PhD thesis
- Jeng MJ, Wung YL, Chang LB, Chow L (2013) Dye-sensitized solar cells with anatase TiO<sub>2</sub> nanorods prepared by hydrothermal method. *Int J Photoenergy* 2013:280253. <https://doi.org/10.1155/2013/280253>
- Kresse G, Furthmüller J (1996) Efficient iterative schemes for ab initio total-energy calculations using a plane-wave basis set. *Phys Rev B* 54:11169–11186. <https://doi.org/10.1103/PhysRevB.54.11169>
- Kresse G, Joubert D (1999) From ultrasoft pseudopotentials to the projector augmented wave method. *Phys Rev B* 59:1758. <https://doi.org/10.1103/PhysRevB.59.1758>
- Kumar R, Sharma P, Mishra PS (2012) A review on the vanillin derivatives showing various biological activities. *Int J PharmTech Res* 4(1):266–279
- Liu Z, Jian Z, Fang J, Xu X, Zhu X, Wu S (2012) Low-temperature reverse microemulsion synthesis, characterization, and photocatalytic performance of nanocrystalline titanium dioxide. *Int J Photoenergy* 2012:8. <https://doi.org/10.1155/2012/702503>
- Mahal H, Badheka L, Mukherjee T (2001) Radical scavenging properties of a flavouring agent-vanillin. *Res Chem Intermed* 27:595–604. <https://doi.org/10.1163/156856701317051699>
- Makula P, Pacia M, Macyk W (2018) How to correctly determine the band gap energy of modified semiconductor photocatalysts based on UV–Vis spectra. *J Phys Chem Lett* 9(23):6814–6817. <https://doi.org/10.1021/acs.jpcl.8b02892>
- Marslin G, Siram K, Maqbool Q, Selvakesavan RK, Kruszka D, Kachlicki P, Franklin G (2018) Secondary metabolites in the green synthesis of metallic nanoparticles. *Materials* 11(6):1–25. <https://doi.org/10.3390/ma11060940>
- Monticone S, Tufeu R, Kanaev A, Scolan E, Sanchez C (2000) Quantum size effect in TiO<sub>2</sub> nanoparticles: does it exist? *Appl Surf Sci* 162–163:565–570. [https://doi.org/10.1016/S0169-4332\(00\)00251-8](https://doi.org/10.1016/S0169-4332(00)00251-8)
- Ochoa Y, Ortegón Y, Rodríguez-Paez JE (2010) Synthesis of TiO<sub>2</sub>, anatase phase by the sol-gel method: study of the effect of the presence of AcacH in the system. *Revista Facultad de Ingeniería Universidad de Antioquia*, pp 29–40
- Pabisiak T, Kiejna A (2007) Energetics of oxygen vacancies at rutile TiO<sub>2</sub> (110) surface. *Solid State Commun* 144(7):324–328. <https://doi.org/10.1016/j.ssc.2007.08.043>
- Rauf MA, Oves M, Rehman FU, Khan AR, Husain N (2019) Bougainvillea flower extract mediated zinc oxide’s nanomaterials for antimicrobial and anticancer activity. *Biomed Pharmacother* 116:108983. <https://doi.org/10.1016/j.biopha.2019.108983>
- Ruhane TA, Islam MT, Rahaman MS, Bhuiyan MMH, Islam JMM, Bhuiyan TI, Khan KA, Khan MA (2017) Impact of photo electrode thickness and annealing temperature on natural dye sensitized solar cell. *Sustain Energy Technol Assess* 20:72–77. <https://doi.org/10.1016/j.seta.2017.01.012>
- Shanavas S, Priyadharsan A, Karthikeyan S, Dharmaboopathi K, Raganvan I, Vidya C, Acevedo R, Anbarasana PM (2019) Green synthesis of titanium dioxide nanoparticles using *Phyllanthus niuri* leaf extract and study on its structural, optical and morphological properties. *Mater Today Proc* 26(4):3531–3534. <https://doi.org/10.1016/j.matpr.2019.06.715>
- Sharma K, Sharma V, Sharma SS (2018) Dye-sensitized solar cells: fundamentals and current status. *Nanoscale Res Lett* 381:1–46. <https://doi.org/10.1186/s11671-018-2760-6>
- Shekarforoush E, Mendes AC, Baj V, Beeren SR, Chronakis IS (2017) Electrospun phospholipid fibers as micro-encapsulation and antioxidant matrices. *Molecules* 22:1708. <https://doi.org/10.3390/molecules22101708>
- Tong T, Zhang J, Tian B, Chen F, He D (2008) Preparation and characterization of anatase TiO<sub>2</sub> microspheres with porous frameworks via controlled hydrolysis of titanium alkoxide followed by hydrothermal treatment. *Mater Lett* 62:2970–2972. <https://doi.org/10.1016/j.matlet.2008.01.085>
- Ünal H, Gunceler D, Güseren O, Ellialtıoglu S, Mete E (2015) Hybrid functional calculated optical and electronic structures of thin anatase TiO<sub>2</sub> nanowires with organic dye adsorbates. *Appl Surf Sci* 354:437–442. <https://doi.org/10.1016/j.apsusc.2015.04.086> (**European Conference on Surface Science 2014**)
- Watson S, Beydoun D, Scott J, Amal R (2004) Preparation of nanosized crystalline TiO<sub>2</sub> particles at low temperature for photocatalysis. *J Nanopart Res* 6:193–207. <https://doi.org/10.1023/B:NANO.0000034623.33083.71>

**Publisher’s Note** Springer Nature remains neutral with regard to jurisdictional claims in published maps and institutional affiliations.